PHYSICAL REVIEW D **84,** 021101(R) (2011)

Measurements of time-dependent CP asymmetries in $B \to D^{*} \mp \pi^{\pm}$ decays using a partial reconstruction technique

S. Bahinipati,[3] K. Trabelsi,[7] K. Kinoshita,[3] K. Arinstein,[1,32] V. Aulchenko,[1,32] T. Aushev,[18,12] A. M. Bakich,[39] V. Balagura,[12] E. Barberio,[22] K. Belous,[11] V. Bhardwaj,[34] B. Bhuyan,[8] M. Bischofberger,[24] A. Bondar,[1,32] A. Bozek,[28] M. Bračko,[20,13] A. Chen,[25] P. Chen,[27] B. G. Cheon,[5] C.-C. Chiang,[27] I.-S. Cho,[50] K. Cho,[15] Y. Choi,[38] J. Dalseno,[21,41] Z. Doležal,[2] Z. Drásal,[2] S. Eidelman,[1,32] N. Gabyshev,[1,32] B. Golob,[19,13] H. Ha,[16] Y. Horii,[44] Y. Hoshi,[43] W.-S. Hou,[27] Y. B. Hsiung,[27] H. J. Hyun,[17] A. Ishikawa,[35] M. Iwabuchi,[50] Y. Iwasaki,[7] T. Iwashita,[24] T. Julius,[22] J. H. Kang,[50] C. Kiesling,[21] H. J. Kim,[17] M. J. Kim,[17] B. R. Ko,[16] N. Kobayashi,[51,45] P. Kodyš,[2] P. Križan,[19,13] T. Kumita,[46] Y.-J. Kwon,[50] S.-H. Kyeong,[50] J. S. Lange,[4] M. J. Lee,[37] S.-H. Lee,[16] J. Li,[6] C. Liu,[36] R. Louvot,[18] A. Matyja,[28] S. McOnie,[39] K. Miyabayashi,[24] H. Miyata,[30] Y. Miyazaki,[23] G. B. Mohanty,[40] M. Nakao,[7] Z. Natkaniec,[28] S. Neubauer,[14] S. Nishida,[7] O. Nitoh,[47] S. Ogawa,[42] T. Ohshima,[23] P. Pakhlov,[12] C. W. Park,[38] M. Petrič,[13] L. E. Piilonen,[48] A. Poluektov,[1,32] M. Röhrken,[14] H. Sahoo,[6] Y. Sakai,[7] O. Schneider,[18] C. Schwanda,[10] A. J. Schwartz,[3] M. E. Sevior,[22] M. Shapkin,[11] C. P. Shen,[6] J.-G. Shiu,[27] P. Smerkol,[13] Y.-S. Sohn,[50] A. Sokolov,[11] E. Solovieva,[12] S. Stanič,[31] M. Starič,[13] K. Sumisawa,[7] T. Sumiyoshi,[46] S. Tanaka,[7] Y. Teramoto,[33] M. Uchida,[51,45] S. Uehara,[7] T. Uglov,[12] Y. Unno,[5] S. Uno,[7] G. Varner,[6] A. Vinokurova,[1,32] C. H. Wang,[26] E. Won,[16] B. D. Yabsley,[39] Y. Yamashita,[29] C. C. Zhang,[9] Z. P. Zhang,[36] P. Zhou,[49] T. Zivko,[13] and A. Zupanc[14]

(The Belle Collaboration)

[1]*Budker Institute of Nuclear Physics, Novosibirsk*
[2]*Faculty of Mathematics and Physics, Charles University, Prague*
[3]*University of Cincinnati, Cincinnati, Ohio 45221*
[4]*Justus-Liebig-Universität Gießen, Gießen*
[5]*Hanyang University, Seoul*
[6]*University of Hawaii, Honolulu, Hawaii 96822*
[7]*High Energy Accelerator Research Organization (KEK), Tsukuba*
[8]*Indian Institute of Technology Guwahati, Guwahati*
[9]*Institute of High Energy Physics, Chinese Academy of Sciences, Beijing*
[10]*Institute of High Energy Physics, Vienna*
[11]*Institute of High Energy Physics, Protvino*
[12]*Institute for Theoretical and Experimental Physics, Moscow*
[13]*J. Stefan Institute, Ljubljana*
[14]*Institut für Experimentelle Kernphysik, Karlsruher Institut für Technologie, Karlsruhe*
[15]*Korea Institute of Science and Technology Information, Daejeon*
[16]*Korea University, Seoul*
[17]*Kyungpook National University, Taegu*
[18]*École Polytechnique Fédérale de Lausanne (EPFL), Lausanne*
[19]*Faculty of Mathematics and Physics, University of Ljubljana, Ljubljana*
[20]*University of Maribor, Maribor*
[21]*Max-Planck-Institut für Physik, München*
[22]*University of Melbourne, School of Physics, Victoria 3010*
[23]*Nagoya University, Nagoya*
[24]*Nara Women's University, Nara*
[25]*National Central University, Chung-li*
[26]*National United University, Miao Li*
[27]*Department of Physics, National Taiwan University, Taipei*
[28]*H. Niewodniczanski Institute of Nuclear Physics, Krakow*
[29]*Nippon Dental University, Niigata*
[30]*Niigata University, Niigata*
[31]*University of Nova Gorica, Nova Gorica*
[32]*Novosibirsk State University, Novosibirsk*
[33]*Osaka City University, Osaka*
[34]*Panjab University, Chandigarh*
[35]*Saga University, Saga*
[36]*University of Science and Technology of China, Hefei*
[37]*Seoul National University, Seoul*

[38]*Sungkyunkwan University, Suwon*
[39]*School of Physics, University of Sydney, NSW 2006*
[40]*Tata Institute of Fundamental Research, Mumbai*
[41]*Excellence Cluster Universe, Technische Universität München, Garching*
[42]*Toho University, Funabashi*
[43]*Tohoku Gakuin University, Tagajo*
[44]*Tohoku University, Sendai*
[45]*Tokyo Institute of Technology, Tokyo*
[46]*Tokyo Metropolitan University, Tokyo*
[47]*Tokyo University of Agriculture and Technology, Tokyo*
[48]*CNP, Virginia Polytechnic Institute and State University, Blacksburg, Virginia 24061*
[49]*Wayne State University, Detroit, Michigan 48202*
[50]*Yonsei University, Seoul*
[51]*Research Center for Nuclear Physics, Osaka*
(Received 4 February 2011; published 5 July 2011)

We report results on time-dependent *CP* asymmetries in $B \to D^{*\mp}\pi^{\pm}$ decays based on a data sample containing 657×10^6 $B\bar{B}$ pairs collected with the Belle detector at the KEKB asymmetric-energy e^+e^- collider at the $\Upsilon(4S)$ resonance. We use a partial reconstruction technique, wherein signal $B \to D^{*\mp}\pi^{\pm}$ events are identified using information only from the fast pion from the B decay and the slow pion from the subsequent decay of the $D^{*\mp}$, where the former (latter) corresponds to $D^{*+}(D^{*-})$ final states. We obtain *CP* violation parameters $S^+ = +0.061 \pm 0.018\,(\text{stat}) \pm 0.012\,(\text{syst})$ and $S^- = +0.031 \pm 0.019\,(\text{stat}) \pm 0.015\,(\text{syst})$.

DOI: 10.1103/PhysRevD.84.021101 PACS numbers: 11.30.Er, 14.40.Nd

In the standard model (SM), *CP* violation occurs due to the presence of a complex phase in the Cabibbo-Kobayashi-Maskawa (CKM) matrix [1]. Precision measurements of the parameters of the CKM matrix are important to investigate new sources of *CP* violation. The study of the time-dependent decay rates of $B^0(\bar{B}^0) \to D^{*\mp}\pi^{\pm}$ provides a method for extracting $\sin(2\phi_1 + \phi_3)$ [2], where ϕ_1 and ϕ_3 [3] are angles of the CKM Unitarity Triangle as defined in [4]. As shown in Fig. 1, these decays can be mediated by both Cabibbo-favored (CF) and doubly-Cabibbo-suppressed (DCS) diagrams, whose amplitudes are proportional to $V_{cb}^* V_{ud}$ and $V_{ub}^* V_{cd}$, respectively, where V_{ij} are the CKM matrix elements and have a relative weak phase difference ϕ_3.

The time-dependent decay rates are given by [5]

$$\begin{aligned} P(B^0 \to D^{*\pm}\pi^{\mp}) &= \frac{1}{8\tau_{B^0}} e^{-|\Delta t|/\tau_{B^0}} [1 \mp C\cos(\Delta m \Delta t) - S^{\pm}\sin(\Delta m \Delta t)], \\ P(\bar{B}^0 \to D^{*\pm}\pi^{\mp}) &= \frac{1}{8\tau_{B^0}} e^{-|\Delta t|/\tau_{B^0}} [1 \pm C\cos(\Delta m \Delta t) + S^{\pm}\sin(\Delta m \Delta t)]. \end{aligned} \tag{1}$$

Here Δt is the difference between the time of the decay and the time that the flavor of the B meson is tagged by the associated B meson; τ_{B^0} is the average neutral B meson lifetime, Δm is the B^0-$\bar{B}^0$ mixing parameter, and $C = (1 - R^2)/(1 + R^2)$, where R is the ratio of the magnitudes of the DCS and CF amplitudes (we assume their magnitudes to be the same for B^0 and $\bar{B}^0$ decays). The *CP* violation parameters for $D^*\pi$ are given by

$$S^{\pm} = \frac{-2R\sin(2\phi_1 + \phi_3 \pm \delta)}{(1 + R^2)}, \tag{2}$$

where δ is the strong phase difference between the CF and DCS amplitudes.

Since the predicted value of R is small, $\sim$0.02 [6], we neglect terms of $\mathcal{O}(R^2)$ (and hence take $C = 1$). The amount of *CP* violation in $D^*\pi$ decays, which is proportional to R, is expected to be small, and hence, a large data sample is needed in order to obtain sufficient sensitivity. To increase statistics, we employ a partial reconstruction technique [7], wherein signal is distinguished from background on the basis of kinematics of the ''fast'' pion (π_f) from the decay $B \to D^*\pi_f$ and the ''slow'' pion (π_s) from the subsequent decay of $D^* \to D\pi_s$; thus the D meson is not reconstructed at all.

Previous analyses have been reported by Belle [8,9] as well as by *BABAR* [10]. This study uses a data sample of 605 fb^{-1} containing 657×10^6 $B\bar{B}$ events. The data

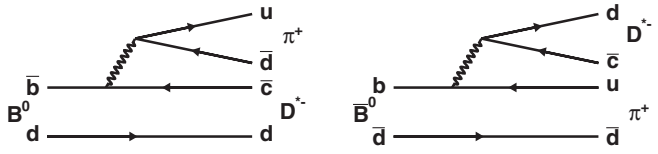

FIG. 1. Diagrams for $B^0 \to D^{*-}\pi^+$ (left) and $\bar{B}^0 \to D^{*-}\pi^+$ (right). Those for $\bar{B}^0 \to D^{*+}\pi^-$ and $B^0 \to D^{*+}\pi^-$ can be obtained by charge conjugation.

sample is about twice the size of the data set used in the previous Belle analysis [9] and supersedes the previous study.

The data were collected with the Belle detector [11] at the KEKB collider [12] operating near the $\Upsilon(4S)$ resonance. The Belle detector is a large-solid-angle magnetic spectrometer that consists of a silicon vertex detector (SVD), a 50-layer central drift chamber (CDC), an array of aerogel threshold Cherenkov counters (ACC), a barrel-like arrangement of time-of-flight scintillation counters (TOF), and an electromagnetic calorimeter (ECL) comprised of CsI(Tl) crystals located inside a superconducting solenoidal coil that provides a 1.5 T magnetic field. An iron flux-return located outside of the coil is instrumented to detect K_L^0 mesons and to identify muons (KLM). A sample containing 152×10^6 $B\bar{B}$ pairs was collected with a 2.0 cm radius beampipe and a 3-layer silicon vertex detector (SVD1), while a sample of 505×10^6 $B\bar{B}$ pairs was collected with a 1.5 cm radius beampipe, a 4-layer silicon vertex detector (SVD2), and a small-cell inner drift chamber [13].

The "signal side" B, decaying to $D^{*+}\pi_f^-$, $D^{*+} \to D^0\pi_s^+$ (or charge conjugate), is reconstructed using pairs of oppositely charged pions. Since the pion originating from the B has a higher momentum in the $\Upsilon(4S)$ c.m. frame than that originating from the D^*, the former (latter) is referred to as the fast (slow) pion. All momenta and energies in this paper are calculated in the $\Upsilon(4S)$ center-of-mass (c.m.) frame, unless otherwise stated. Fast pion candidates are required to have a radial (longitudinal) impact parameter $dr < 0.1$ cm ($|dz| < 2.0$ cm) and to have associated hits in the SVD. We reject leptons and kaons based on information from the CDC, TOF and ACC. A requirement is made on the fast pion momentum, $1.93\ \mathrm{GeV}/c < p_f < 2.50\ \mathrm{GeV}/c$. Soft pion candidates are required to have momenta in the range $0.05\ \mathrm{GeV}/c < p_s < 0.30\ \mathrm{GeV}/c$. No particle identification requirement is applied for these pions. We impose only a loose requirement that they originate from the run-dependent interaction point (IP) profile. The IP has $\sigma_z \sim 4$ mm along the beam direction (z), and $\sigma_x \sim 100$ μm and $\sigma_y \sim 10$ μm in the plane perpendicular to the beam direction.

For any given π_f from a signal B decay, the energy of the D^* may be known through energy conservation, $E_{D^*} = E_B - E_{\pi_f}$, where $E_B = \sqrt{s}/2$ at the $\Upsilon(4S)$. The magnitude of the momentum is then $|\vec{p}_{D^*}| = \sqrt{E_{D^*}^2 - m_{D^*}^2}$. Because the B meson is slow in the c.m. frame, its momentum $|\vec{p}_B| = \sqrt{E_B^2 - m_{B^0}^2} \approx 0.3\ \mathrm{GeV}/c$ is small relative to the π_f and D^* momenta. It follows from momentum conservation

$$\vec{p}_{D^*} = \vec{p}_B - \vec{p}_{\pi_f} \tag{3}$$

that the direction of the D^* momentum can be approximated as the direction opposite to $\vec{p}_{\pi_f}$. This approximate D^* four-momentum is denoted as the "partially reconstructed" D^*. We define a quantity $p_\delta = |\vec{p}_{\pi_f}| - |\vec{p}_D^*|$, which for signal decays satisfies $|p_\delta| \leq |\vec{p}_B|$, as can be seen by examining Eq. (3).

We then examine the soft pion after boosting it into the partially reconstructed D^* frame; in the true D^* rest frame, the soft pion is monoenergetic and its momentum has an angular distribution characteristic of a pseudoscalar to pseudoscalar-vector transition, $\propto \cos^2\theta$ where θ is taken relative to the boost axis. In the partially reconstructed frame, the momentum will have a limited spread. We study the components parallel and perpendicular to the boost axis, denoted $p_\parallel$ and $p_\perp$, respectively.

We use the three kinematic variables p_δ, $p_\parallel$ and $p_\perp$ to distinguish between signal and background. Background events are separated into three categories: $D^{*\mp}\rho^\pm$, which is kinematically similar to the signal; correlated background, in which the soft pion originates from the decay of a D^* that in turn originates from the decay of the same B as the fast pion candidate, excluding $D^{*\mp}\pi^\pm$ and $D^{*\mp}\rho^\pm$ decays (e.g., $B \to D^{**}\pi$, $B \to D^* a_1$, $B \to D^* l\nu$); and uncorrelated background, which includes all other background sources (e.g., continuum processes, $B \to D\pi$). The distributions of the kinematic variables for signal and background categories are determined from a large sample of Monte-Carlo (MC) generated data corresponding to 3 times the integrated luminosity of our data sample.

We retain candidates that satisfy $-0.10\ \mathrm{GeV}/c < p_\parallel < 0.07\ \mathrm{GeV}/c$, $-0.60\,\mathrm{GeV}/c < p_\delta < 0.50\,\mathrm{GeV}/c$, and $p_\perp < 0.05\ \mathrm{GeV}/c$. In the cases where more than one candidate satisfies these criteria, we select the one with the largest value of $\delta_{\pi_f\pi_s}$, where $\delta_{\pi_f\pi_s}$ is the angle between the fast pion direction and the soft pion direction in the $\Upsilon(4S)$ c.m. frame. The signal region is defined as $-0.40\,\mathrm{GeV}/c < p_\delta < 0.40\,\mathrm{GeV}/c$, $-0.05\,\mathrm{GeV}/c < p_\parallel < -0.01\,\mathrm{GeV}/c$ or $0.01\ \mathrm{GeV}/c < p_\parallel < 0.04\ \mathrm{GeV}/c$, and $p_\perp < 0.05\ \mathrm{GeV}/c$.

The determination of the flavor of the B meson opposite to the signal side B, which we refer as the tag-side B, is essential for this measurement. In order to tag the flavor of the associated B meson, we require the presence of a high-momentum lepton (l) in the event. This helps reduce background from continuum $e^+e^- \to q\bar{q}(q = u, d, s, c)$ processes. Tagging lepton candidates are required to be positively identified either as electrons, on the basis of information from the CDC, ECL, and ACC, or as muons, on the basis of information from the CDC and the KLM. They are required to have momenta in the range $1.1\ \mathrm{GeV}/c < p_l < 2.3\ \mathrm{GeV}/c$, and to have an angle with the fast pion candidate that satisfies $\cos\delta_{\pi_f l} > -0.75$ in the $\Upsilon(4S)$ c.m. frame. These requirements reduce to a negligible level (0.7%) the contribution of leptons produced from semileptonic decays of the unreconstructed D mesons in the $B \to D^{*\mp}\pi^\pm$ decay chain.

Vertexing requirements identical to those for the fast pion are applied to the lepton candidate in order to obtain

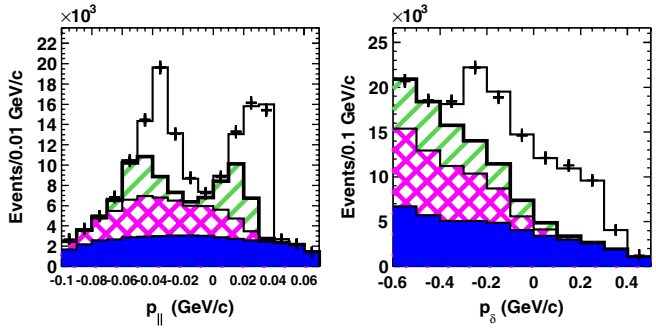

FIG. 2 (color online). Results of the fits to $D^*\pi$ candidates projected onto $p_\parallel$ (left) and p_δ (right) in the signal region of the two kinematic variables. The contributions are $D^*\pi$ (open), $D^*\rho$ (green slanted lines), correlated background (magenta crossed lines), and uncorrelated background (shaded blue). Data are shown as points with error bars.

an accurate vertex position. To further suppress the remaining small continuum background, we impose a loose requirement on the ratio of the second to zeroth Fox-Wolfram [14] moments, $R_2 < 0.6$.

Event-by-event signal and background fractions are determined from binned maximum likelihood fits to the two-dimensional distributions of p_δ and $p_\parallel$. The results of these fits, projected onto each of the two variables, are shown in Fig. 2, and summarized in Table I. We obtain a purity of $59.0 \pm 0.4\%$ in the signal region, where purity is defined as the ratio of the signal to total yields.

At the KEKB asymmetric-energy e^+e^- (3.5 GeV on 8 GeV) collider, operating at the $\Upsilon(4S)$ resonance ($E_{\rm c.m} = 10.58$ GeV), the $\Upsilon(4S)$ is produced with a Lorentz boost of $\beta\gamma = 0.425$, almost along the electron beam line (z). In the $\Upsilon(4S)$ c.m, B^0 and $\bar{B}^0$ mesons are approximately at rest. Hence the proper time difference (Δt) between the signal side vertex ($z_{\rm sig}$) and the tag-side vertex ($z_{\rm tag}$) is obtained from the fast pion on the signal side and the tagging lepton. The variable Δt is defined as

$$\Delta t \approx (z_{\rm sig} - z_{\rm tag})/\beta\gamma c. \tag{4}$$

$z_{\rm sig}$ is obtained from the intersection of the fast pion's track and the IP, and $z_{\rm tag}$ is obtained from the intersection of the tagging lepton's track and the IP.

To measure the CP violation parameters, we perform a simultaneous unbinned fit to four samples: two are of same-flavor (SF) events, namely, $\pi^+ l^+$, $\pi^- l^-$, in which the fast pion and the tagging lepton have the same charge, and the other two are of opposite-flavor (OF) events, namely, $\pi^+ l^-$, $\pi^- l^+$, in which the fast pion and the tagging lepton have opposite charge. We minimize the quantity $-\ln\mathcal{L} = -\sum_i \ln\mathcal{L}_i$, where

$$\mathcal{L}_i = f_{D^*\pi}P_{D^*\pi} + f_{D^*\rho}P_{D^*\rho} + f_{\rm unco}P_{\rm unco} + f_{\rm corr}P_{\rm corr}. \tag{5}$$

Here, f_x stands for the event-by-event fraction from source x and is obtained from the fits to the kinematic variables, and P denotes the probability density functions (PDFs) for signal and backgrounds, which contain an underlying physics PDF with experimental effects taken into account. The convolution of the physics PDF with experimental effects will be described later. For $D^*\pi$ and $D^*\rho$, the PDF is given by Eq. (1), where for $D^*\rho$ the $S^\pm$ terms are effective parameters averaged over the helicity states [15] and are constrained to be zero. The PDF for correlated background contains a term for neutral B decays (given by Eq. (1) with $S^\pm = 0$) and a term for charged B decays (for which the PDF is $\frac{1}{2\tau_{B^+}} e^{-|\Delta t|/\tau_{B^+}}$, where τ_{B^+} is the lifetime of the charged B meson). The PDF for uncorrelated background also contains neutral and charged B components, with the remainder from continuum $e^+e^- \to q\bar{q}$ ($q = u, d, s, c$) processes. The continuum PDF is modeled with two components: one with negligible lifetime, and the other with a finite lifetime, which takes into account the dependence of average lifetime of the charm contribution in the continuum (close to the average D meson lifetime).

The parameters in $P_{\rm unco}$ and $P_{\rm corr}$ are obtained from separate simultaneous fits to OF and SF candidates in the respective sideband regions, defined later. Since there is no CP violation in background, the corresponding parameters are fixed to zero in these fits. The fit is further simplified by fixing the biases in Δz to zero (discussed later in detail). MC simulation studies demonstrate that varying or fixing these biases to zero does not affect the background parameters.

To measure the uncorrelated background shape, we use events in a sideband region, $-0.10\ {\rm GeV}/c < p_\parallel < +0.07\ {\rm GeV}/c$, $-0.60\ {\rm GeV}/c < p_\delta < 0.50\ {\rm GeV}/c$, and $0.08\ {\rm GeV}/c < p_\perp < 0.10\ {\rm GeV}/c$, which is populated mostly by uncorrelated background ($\sim 90\%$). To determine the correlated background parameters, we use events in a sideband region, $-0.10\,{\rm GeV}/c < p_\parallel < -0.07\,{\rm GeV}/c$, $-0.60\ {\rm GeV}/c < p_\delta < 0.00\ {\rm GeV}/c$, and $0.00\ {\rm GeV}/c < p_\perp < 0.05\ {\rm GeV}/c$. This sideband region is dominated by both correlated and uncorrelated backgrounds and has a very small amount of $D^*\pi$ signal and $D^*\rho$ background. The uncorrelated background parameters are fixed to the values obtained in the previous fit. Figure 3 shows $p_\perp$ distributions for signal and various background components in MC simulations, corresponding to about 3 times the size of the data.

The PDF for signal and background in Eq. (5) must be convolved with the corresponding Δz resolution functions related to the kinematic smearing ($\mathcal{R}_k$), detector resolution ($\mathcal{R}_{\rm det}$), and asymmetry in Δz from nonprimary tracks

TABLE I. Summary of the yields in the signal region.

$D^*\pi$	$50\,196 \pm 286$
$D^*\rho$	$10\,232 \pm 150$
Correlated background	$10\,425 \pm 135$
Uncorrelated background	$14\,193 \pm 128$

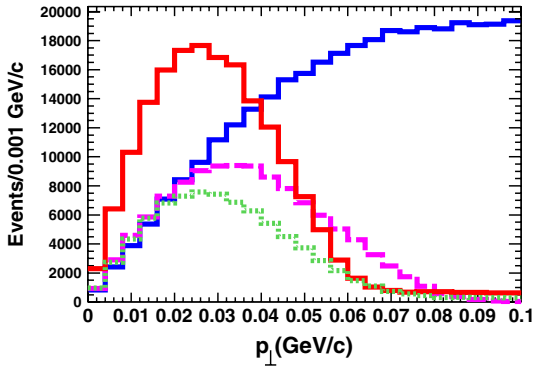

FIG. 3 (color online). $p_\perp$ distributions for various MC simulations, showing the following contributions: $D^*\pi$ (red solid line), $D^*\rho$ (dotted green line), correlated background (dashed magenta line), and uncorrelated background (blue solid line).

($\mathcal{R}_{\rm np}$). The resolution function related to kinematic smearing is due to the fact that we use the approximation of Eq. (4). The detector resolution and smearing due to the asymmetry in Δz from nonprimary tracks are described in detail elsewhere [9].

To account for mistagging, the PDFs in Eq. (5) are divided into two components

$$P(l^{\mp}, \pi_f^{\pm}) = (1 - w_{\mp})P(B^0/\bar{B}^0 \to D^{*\mp}\pi^{\pm}) + w_{\pm}P(\bar{B}^0/B^0 \to D^{*\mp}\pi^{\pm}), \quad (6)$$

where w^+ and w^- are the wrong-tag fractions, defined as the probabilities to incorrectly measure the flavor of tagged B^0 and $\bar{B}^0$ mesons, respectively, and are determined from the data as free parameters in the fit for $S^{\pm}$.

The time difference Δt is related to the measured quantity Δz as described in Eq. (4), with an additional term due to possible offsets in the mean value of Δz,

$$\Delta t \to \Delta t + \epsilon_{\Delta t} \simeq (\Delta z + \epsilon_{\Delta z})/\beta\gamma c. \quad (7)$$

It is essential to allow nonzero values of $\epsilon_{\Delta t}$ since a small bias can mimic the effect of *CP* violation:

$$\cos(\Delta m \Delta t) \to \cos(\Delta m \Delta t) - \Delta m \epsilon_{\Delta t} \sin(\Delta m \Delta t). \quad (8)$$

A bias as small as $\epsilon_{\Delta z} \sim 1$ μm can lead to sinelike terms as large as 0.01, comparable to the expected size of the *CP* violation effect. Because both vertex positions are obtained from single tracks, the partial reconstruction analysis is more susceptible than other Belle *CP* violation analyses to such biases. We allow separate offsets for Δz for each combination of π_f and l charges. Thus we have eight offsets in total, four for each data sample, SVD1 and SVD2.

To extract the *CP* violation parameters we fix τ_{B^0} and Δm at their world average values ($\tau_{B^0} = 1.530 \pm 0.009$ ps and $\Delta m = 0.507 \pm 0.005$ ps^{-1} [4]), and fit with S^+, S^-, two wrong tag fractions, and eight offsets as free parameters. We obtain $S^+ = +0.061 \pm 0.018$ and $S^- = +0.031 \pm 0.019$, where the errors are statistical only. The correlation coefficient parameter between S^+ and S^- is consistent with 0. The wrong tag fractions are $w_- = (5.3 \pm 0.3)\%$ and $w_+ = (5.2 \pm 0.3)\%$. All floating offsets are consistent with zero except for one of the OF combinations ($\pi_f = \pi^-$, $l = \ell^+$) in the SVD1 sample. The results are shown in Fig. 4. Using large MC samples generated with nonzero and zero $S^{\pm}$ values, we do not find any significant bias in the procedure.

To further illustrate the *CP* violation effect, we define asymmetries in the same flavor events ($\mathcal{A}^{\rm SF}$) and in the opposite flavor events ($\mathcal{A}^{\rm OF}$) as

$$\mathcal{A}^{\rm SF} = \frac{N_{\pi^- l^-}(\Delta z) - N_{\pi^+ l^+}(\Delta z)}{N_{\pi^- l^-}(\Delta z) + N_{\pi^+ l^+}(\Delta z)},$$
$$\mathcal{A}^{\rm OF} = \frac{N_{\pi^+ l^-}(\Delta z) - N_{\pi^- l^+}(\Delta z)}{N_{\pi^+ l^-}(\Delta z) + N_{\pi^- l^+}(\Delta z)}, \quad (9)$$

where the N values denote the number of events for each combination of f and l charge. These are shown in Fig. 5.

This analysis is very sensitive to the vertexing bias. Hence, we include Δz offsets in the fits to account for this bias. In order to estimate the error due to these offsets, we perform fits to obtain $S^{\pm}$ values with and without offsets using an ensemble of 100 generated $D^*\pi$ signal samples and use the difference between the two results as the systematic error. We obtain negligible contribution to the systematic errors when we float Δz offsets in the background PDF.

Other sources of systematic error are the resolution functions, $\mathcal{R}_k$, $\mathcal{R}_{\rm det}$, and $\mathcal{R}_{\rm np}$, uncorrelated and correlated backgrounds and physics parameters, Δm, τ_{B^0}, and τ_{B^+} that are fixed in the fit to extract $S^{\pm}$. The parameters of the resolution functions and backgrounds are varied by $\pm 1\sigma$

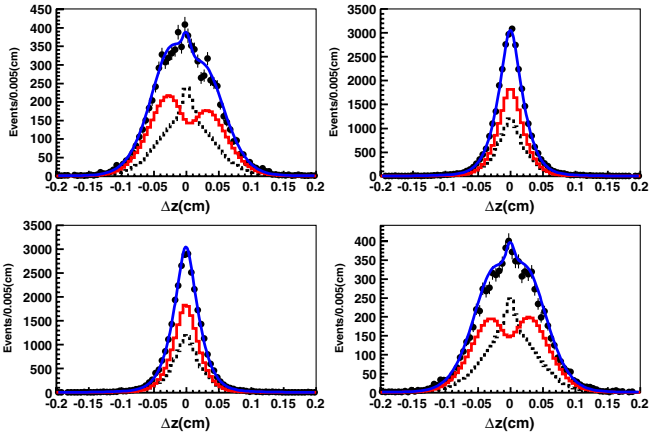

FIG. 4 (color online). Δz distributions for four flavor-charge combinations: $\pi^- l^-$ (top left), $\pi^- l^+$ (top right), $\pi^+ l^-$ (bottom left), and $\pi^+ l^+$ (bottom right). The fit result (solid blue line) is superimposed on the data (solid points with error-bars). The signal and background components are shown as the solid red and dotted black curves, respectively.

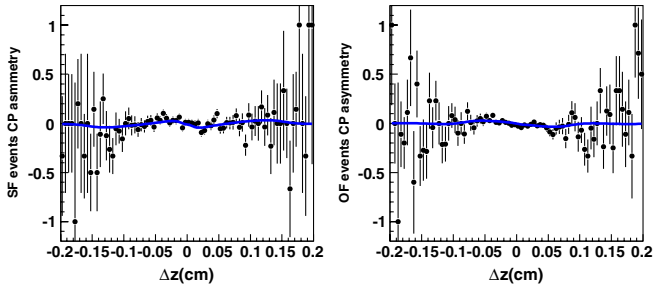

FIG. 5 (color online). Results of the fit to obtain S^+ and S^-, shown as asymmetries in the SF events (left) and OF events (right). The fit results (solid blue lines) are superimposed on the data.

(with Δm and τ_{B^0} fixed), respectively, where σ's are the corresponding errors of the parameters and the difference is assigned as systematic error. We vary the physics parameters by $\pm 1\sigma$, where σ is the error of the corresponding Particle Data Group values, and we then use the difference between the $S^{\pm}$ values thus obtained and the default values as the systematic error. When the fit is performed floating $S^{\pm}$ values, along with τ_{B^0} and Δm, we obtain $S^+ = +0.055 \pm 0.018$ and $S^- = +0.039 \pm 0.019$, $\tau_{B^0} = 1.550 \pm 0.008$ ps and $\Delta m = 0.473 \pm 0.004$ ps^{-1}, where the errors are statistical only. The deviations from the nominal fit (0.06, 0.08) are close to the systematic errors assigned for the physics parameters (Table II). The difference between the $S^{\pm}$ values obtained floating both Δm and τ_{B^0} parameters and the default value is also added to the systematic error estimation. In the fits to extract $S^{\pm}$, $S^{\pm}{}_{D^*\rho}$ and $S^{\pm}{}_{\rm corr}$ are set to zero. For the systematic error due to these parameters, the fit is performed with these values set to ± 0.05 and the difference between the $S^{\pm}$ value thus obtained and the default value is assigned as the systematic error.

We use a triple Gaussian to model the detector resolution ($R_{\rm det}$) function. We consider the systematic uncertainty due to the lack of knowledge of the exact functional form of the resolution model. When the resolution models are varied, we obtain shifts as large as 0.006 for S^+. This is conservatively assigned as the systematic error due to this source.

We obtain a vertexing systematic error of 0.003 for $S^{\pm}$. Additional systematic errors result from varying the number of bins for the kinematic variables, p_δ and $p_\parallel$ in the yield fit.

The systematic errors are summarized in Table II. The total systematic error is obtained by adding the above terms in quadrature.

In conclusion, we have measured *CP* violation parameters that depend on ϕ_3 using the time-dependent decay rates of $B^0 \to D^{*\mp}\pi^{\pm}$ with a data sample containing 657×10^6 $B\bar{B}$ events. We determine the *CP* violation parameters $S^{\pm}$ to be

TABLE II. Summary of possible sources of systematic error.

Systematic error source	S^+	S^-
Δz offset	0.002	0.003
$\mathcal{R}_k$ parameters	0.002	0.003
$\mathcal{R}_{\rm det}$ parameters	0.002	0.002
$\mathcal{R}_{np}$ parameters	0.004	0.004
Background parameters	0.001	0.001
Physics parameters	0.006	0.009
Floating τ_{B^0} and Δm	0.006	0.008
Yield fit	0.003	0.005
Resolution model	0.006	0.002
IP constraint	0.003	0.003
Total systematic error	0.012	0.015

$$\begin{aligned} S^+ &= +0.061 \pm 0.018 \pm 0.012, \\ S^- &= +0.031 \pm 0.019 \pm 0.015, \end{aligned} \tag{10}$$

where the first errors are statistical and the second errors are systematic. We can also express the results as parameters a, c, defined as

$$a = -(S^+ + S^-)/2, \qquad c = -(S^+ - S^-)/2. \tag{11}$$

Our results thus become

$$\begin{aligned} a &= -0.046 \pm 0.013 \pm 0.015, \\ c &= -0.015 \pm 0.013 \pm 0.015. \end{aligned} \tag{12}$$

The deviation of a from zero is a measure of the amount of *CP* violation. We obtain a significance of 2.5σ on the *CP* violation parameter, a. Our measurement is consistent with the world average value and significantly improves the precision of previous measurements reported by Belle [8,9] as well as by *BABAR* [10] and supersedes our earlier result [9].

We thank the KEKB group for excellent operation of the accelerator, the KEK cryogenics group for efficient solenoid operations, and the KEK computer group and the NII for valuable computing and SINET3 network support. We acknowledge support from MEXT, JSPS and Nagoya's TLPRC (Japan); ARC and DIISR (Australia); NSFC (China); MSMT (Czechia); DST (India); MEST, NRF, NSDC of KISTI, and WCU (Korea); MNiSW (Poland); MES and RFAAE (Russia); ARRS (Slovenia); SNSF (Switzerland); NSC and MOE (Taiwan); and DOE (USA).

[1] M. Kobayashi and T. Maskawa, Prog. Theor. Phys. **49**, 652 (1973); N. Cabibbo, Phys. Rev. Lett. **10**, 531 (1963).
[2] I. Dunietz and R. G. Sachs, Phys. Rev. D **37**, 3186 (1988); **39**, 3515(E) (1989); I. Dunietz, Phys. Lett. B **427**, 179 (1998).
[3] ϕ_1 and ϕ_3 are sometimes referred to as β and γ.
[4] K. Nakamura *et al.* (Particle Data Group), J. Phys. G **37**, 075021 (2010).
[5] R. Fleischer, Nucl. Phys. B **671**, 459 (2003).
[6] D. A. Suprun, C.-W. Chiang, and J. L. Rosner, Phys. Rev. D **65**, 054025 (2002).
[7] Y. Zheng *et al.* (Belle Collaboration), Phys. Rev. D **67**, 092004 (2003).
[8] T. Gershon *et al.* (Belle Collaboration), Phys. Lett. B **624**, 11 (2005).
[9] F. J. Ronga *et al.* (Belle Collaboration), Phys. Rev. D **73**, 092003 (2006).
[10] B. Aubert *et al.* (*BABAR* Collaboration), Phys. Rev. D **71**, 112003 (2005).
[11] A. Abashian *et al.* (Belle Collaboration), Nucl. Instrum. Methods Phys. Res., Sect. A **479**, 117 (2002).
[12] S. Kurokawa and E. Kikutani, Nucl. Instrum. Methods Phys. Res., Sect. A **499**, 1 (2003), and other papers included in this Volume.
[13] Z. Natkaniec *et al.* (Belle SVD2 Group), Nucl. Instrum Methods Phys. Res., Sect. A **560**, 1 (2006).
[14] G. C. Fox and S. Wolfram, Phys. Rev. Lett. **41**, 1581 (1978).
[15] N. Sinha and R. Sinha, Phys. Rev. Lett. **80**, 3706 (1998); D. London, N. Sinha, and R. Sinha, Phys. Rev. Lett. **85**, 1807 (2000).